16TH EUROPEAN CONFERENCE ON EARTHQUAKE ENGINEERING THESSALONIKI 18 - 21 JUNE 2018

# SEISMIC IMPACT AND DESIGN OF BURIED PIPELINES

Timo SCHMITT[1], Julia ROSIN[2], Christoph BUTENWEG[3]

## ABSTRACT

Seismic design of buried pipeline systems for energy and water supply is not only important for plant and operational safety but also for the maintenance of the supply infrastructure after an earthquake.
The present paper shows special issues of the seismic wave impacts on buried pipelines, describes calculation methods, proposes approaches and gives calculation examples. This paper regards the effects of transient displacement differences and resulting tensions within the pipeline due to the wave propagation of the earthquake. However, the presented model can also be used to calculate fault rupture induced displacements.
Based on a three-dimensional Finite Element Model parameter studies are performed to show the influence of several parameters such as incoming wave angle, wave velocity, backfill height and synthetic displacement time histories. The interaction between the pipeline and the surrounding soil is modeled with non-linear soil springs and the propagating wave is simulated affecting the pipeline punctually, independently in time and space.
Special attention is given to long-distance heat pipeline systems. Here, in regular distances expansion bends are arranged to ensure movements of the pipeline due to high temperature. Such expansion bends are usually designed with small bending radii, which during the earthquake lead to high bending stresses in the cross-section of the pipeline. Finally, an interpretation of the results and recommendations are given for the most critical parameters.

*Keywords: buried pipeline; earthquake; seismic impact; transient displacement*

## 1. INTRODUCTION

Pipeline systems are a part of the critical infrastructure. Past earthquakes have shown the vulnerability of pipeline systems. After the Kobe earthquake in Japan in 1995 for instance, in some regions the water supply was interrupted for almost two months. Buried pipelines are exposed to different effects of seismic impacts. In the following, effects of seismic wave impact due to transient displacement differences within the pipeline resulting from seismic wave propagation are described and studied performing small example calculations. Other impacts are permanent displacements due to fault rupture displacements at the surface, soil liquefaction, landslides and seismic soil compaction.
For the examples shown later, a three-dimensional Finite Element Model with non-linear soil springs is used. The seismic impact, a propagating wave, is simulated by displacement time histories, affecting different points of the pipeline independently in time and space. The resulting stresses mainly are caused by displacement differences of neighboring pipeline segments and by soil-structure interaction. The calculation examples focus on pipeline bends as the most critical parts. Therefore, Kármán's elasticity factors as well as the stress intensity factors for curved pipe sections should be considered. The seismic verification of the pipeline for wave propagation in the soil can be achieved by observing normative strain criteria.

[1]Dr. Timo Schmitt, Structures and Seismology, TÜV SÜD Industrie Service GmbH, Munich, Germany, timo.schmitt@tuev-sued.de
[2]Dr. Julia Rosin, SDA-engineering GmbH, Herzogenrath, Germany, rosin@sda-engineering.de
[3]Prof. Dr. Christoph Butenweg, Energy Technology, FH Aachen University of Applied Sciences, Jülich, Germany, christoph.butenweg@fh-aachen.de

## 2. SEISMIC WAVE IMPACT ON PIPELINES

The rupture process of an earthquake results in seismic waves, which propagate from the earthquake source to the earth´s surface. The wave propagation causes soil particle movements and thus displacements in the ground, which impact on buried pipelines. This results in seismic stresses in the pipelines and can lead to serious damage to the pipes, if not taken into account. For the determination of the deformations due to seismic wave action, it is necessary to consider the impact of the different wave types. From the earthquake source the body waves are spread out. They are divided into P waves (primary waves, longitudinal waves or compression waves) and slower S waves (secondary waves, transverse waves or shear waves). The S-waves are of particularly importance for the design of buildings due to the almost horizontal direction of action and the larger amplitudes. The reflection of the body waves at the earth´s surface and their superposition result in surface waves. It is distinguished between Love waves (L waves) and Rayleigh waves (R waves).

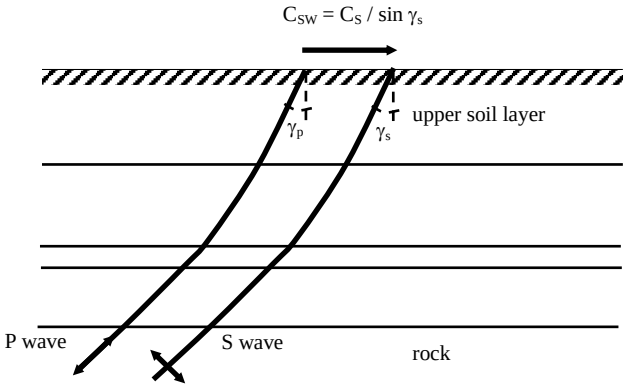


Figure 1. Wave paths of P and S wave, angle of incidence $\gamma_s$, $\gamma_p$ and apparent wave velocity $C_{SW}$ at the earth´s surface

Since buried pipelines are located close to the earth´s surface, the angle between the wave path of the body waves and the surface has a significant influence on the expected ground movements. Figure 1 shows the wave paths and directions of action of the P and S waves in a vertical section. The P waves act in the direction of the wave path, while the S waves are orthogonal to the P waves. Along the travel path of the waves to the earth´s surface, the path becomes increasingly steeper due to the upward decreasing density of the soil layers. The angles of incidence $\gamma_p$ (P wave) and $\gamma_s$ (S wave) to the earth´s surface are usually very small. Therefore, often horizontally polarized S waves ($\gamma_s = 0$) are assumed for soil dynamic calculations.

The propagation velocity of the waves along the earth´s surface essentially depends on the angle of incidence of the waves and is called apparent wave velocity. The apparent wave velocity $C_{SW}$ of the shear wave along the earth´s surface can be calculated by $C_{SW} = C_S / \sin \gamma_s$ (see Figure 1). For $\gamma_s = 0°$ the earthquake wave comes in vertically from below (vertically polarized S wave, $C_{SW} = \infty$). In this case, theoretically all points along the pipe are simultaneously excited resulting in no relative displacements. According to O´Rourke et al. (1982), observed apparent wave velocities are in the range between 2 and 5 km / s, with the mean value around 3.5 km / s.

## 3. CALCULATION MODEL

The following parametric study is executed using a three-dimensional Finite-Element model in which the pipeline is represented by thin-walled beam elements. The interactions of the beam elements with the surrounding soil are modelled by non-linear spring elements in longitudinal, transversal and vertical direction. Inertia effects of the pipeline are not considered (Figure 2).

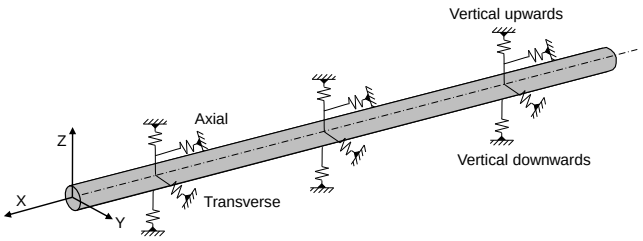


Figure 2. Model of the pipeline with non-linear springs

Two springs in vertical direction are applied to describe the movements upwards and downwards with different stiffness properties. The spring-characteristics of the soil are calculated according to the guidelines provided by ASCE (1984) and ALA (2001). The formulas for the calculation are briefly described in the following.

### *3.1 Spring-Characteristic in Axial Direction*

The spring-characteristic in axial direction is illustrated in Figure 3. The characteristic in axial direction is described by means of the maximum axial force $T_u$ and the maximum relative displacement $\Delta_t$. The maximum transferable force $T_u$ per unit length in axial direction can be calculated as follows:

$$T_u = \pi \cdot D \cdot \alpha \cdot c + \pi \cdot D \cdot H \cdot \gamma \frac{1+K_0}{2} \tan(f \cdot \varphi) \tag{1}$$

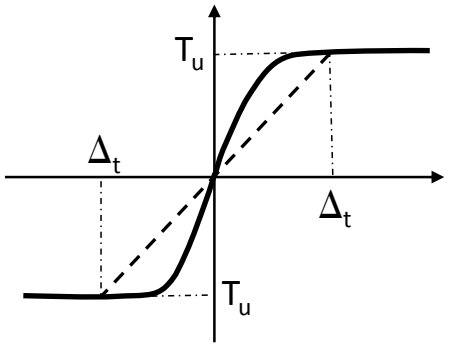


Figure 3. Spring characteristic in axial direction

Where D [m] is the pipe diameter, c [kN/m²] is the cohesion, $\alpha$ [-] is the factor for adhesion, H [m] is the backfill height above the pipe, $K_0$ [-] is the coefficient for earth pressure at rest, $\gamma$ [kN/m²] is the effective soil weight, f [-] is the coefficient for the consideration of the pipe material (concrete: 1.0; smooth steel: 0.7) and $\varphi$[°] is the angle of friction of the soil. The factor of adhesion $\alpha$ is defined as follows:

$$\alpha = 0{,}608 - 0{,}00123 \cdot c - \frac{0{,}274}{\left(\frac{c}{100}\right)^2 + 1} + \frac{0{,}695}{\left(\frac{c}{100}\right)^3 + 1} \tag{2}$$

The maximum relative displacement $\Delta_t$ is equal to 3 mm for densely packed sand, 5 mm for loose sand, 8 mm for stiff cohesive soil and 10 mm for soft cohesive soil.

### *3.2 Spring-Characteristic in Transversal Direction*

Figure 4 depicts the spring characteristic in transverse direction, which is defined by the maximum force $P_u$ in transverse direction and the maximum relative displacement $\Delta_p$.

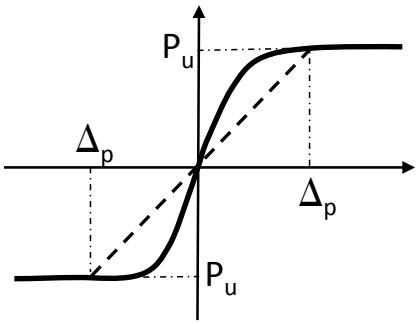


Figure 4. Spring characteristic in transverse direction

The maximum force in transverse direction $P_u$ per unit length can be calculated by:

$$P_u = N_{ch} \cdot c \cdot D + N_{qh} \cdot \bar{\gamma} \cdot H \cdot D \tag{3}$$

$N_{ch}$ is the horizontal load bearing factor for cohesive soils (0 for c = 0) and $N_{qh}$ for sand (0 for φ = 0). The two load bearing factors are shown in Figure 5. The relative displacement $\Delta_p$ associated with the maximum force $P_u$ is equal to 0.07 to 0.1 (H + D/2) for loose sand, 0.03 to 0.05 (H + D/2) for medium dense sand, 0.02 to 0.03 (H + D/2) for dense sand and 0.03 to 0.05 (H + D/2) for stiff to cohesive soil.

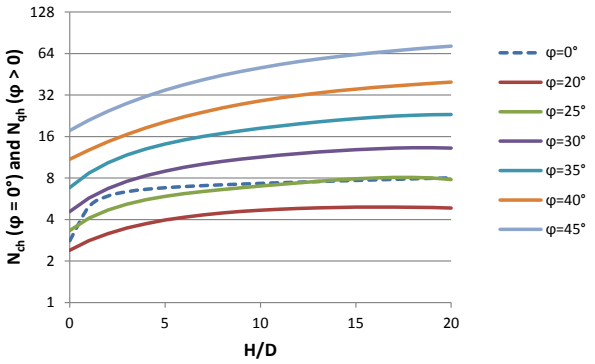


Figure 5. Load bearing factors $N_{qh}$ and $N_{ch}$ (ALA 2001)

### *3.3 Spring-Characteristic in Vertical Direction*

The spring characteristic in vertical direction (Figure 6) is defined by the maximum transferable axial force $Q_u$ / $Q_d$ and the maximum relative displacement $\Delta_{qu}$ / $\Delta_{qd}$. The maximum vertical force per unit length $Q_u$ for upward movements is defined by:

$$Q_u = N_{cv} \cdot c \cdot D + N_{qv} \cdot \bar{\gamma} \cdot H \cdot D \tag{4}$$

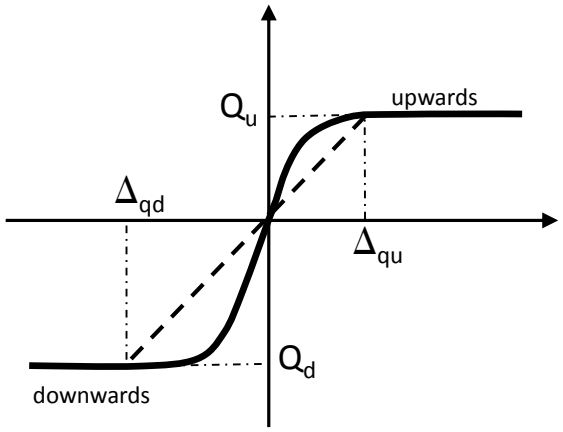


Figure 6. Spring characteristic in vertical direction

$N_{cv}$ is the vertical load bearing factor for cohesive soils (0 for c = 0) and $N_{qv}$ for sand (0 for φ = 0), which can be calculated as follows:

$$N_{cv} = 2\left(\frac{H}{D}\right) \leq 10 \tag{5}$$

applicable for: $\left(\frac{H}{D}\right) \leq 10$

$$\mathrm{N_{qv}} = \left(\frac{\varphi \cdot \mathrm{H}}{44 \cdot \mathrm{D}}\right) \leq \mathrm{N_q} \tag{5}$$

The relative displacement $\Delta_{qu}$ for the maximum vertical spring force $Q_u$ is 0.01 H to 0.02 H and < 0.1 D for loose to densely packed sand and 0.1 H to 0.2 H and < 0.2 D for stiff to soft cohesive soil. The maximum vertical force $Q_d$ per unit length for upward movements is:

$$Q_d = N_c \cdot c \cdot D + N_q \cdot \gamma \cdot H \cdot D + N_\gamma \cdot \bar{\gamma} \cdot \frac{D}{2}, \tag{6}$$

Where $\bar{\gamma}$ [kN/m³] is the total soil weight and $N_c$, $N_q$ and $N_\gamma$ are the vertical load bearing factors as a function of the angle of friction of the soil (ASCE 1984). The relative displacement $\Delta_{qd}$ corresponding to the maximum vertical force $Q_d$ is 0.1 D to 0.15 D for non-cohesive and cohesive soil.

### *3.4 Spring Law for Torsion*

The resistance of the soil against rotations of the pipe around the longitudinal axis is not described in the guidelines ASCE (1984) and ALA (2001). However, it seems reasonable that the torsional resistance shall be considered in curved sections of the pipeline. According to Kuhlmann (2004), the assumption can be made that the same resistance as for relative movements in the tangential direction can be assumed in axial direction. With the maximum transferable axial force $T_u$ per unit length (Eq. 1), the maximum torsional moment $R_u$ per unit of length can be calculated as follows:

$$R_u = T_u \cdot \frac{D}{2} \tag{7}$$

As before, a bilinear spring characteristic is applied to describe the torsional spring characteristic. The relative rotation $\Delta\varphi$ needed to activate the maximum torsional resistance $R_u$ can be calculated by converting the relative displacement $\Delta_t$, which activates the maximum axial ground resistance, in radians:

$$\Delta\varphi = \frac{2 \cdot \Delta_t}{D} \tag{8}$$

## 4 SEISMIC IMPACT LOADS

In the three-dimensional calculation model, the seismic impact is applied as displacement time histories in the three spatial directions on the supporting points of the spring elements. The wave propagation then is simulated by the time-delayed application of the seismic action at the supporting points corresponding to the apparent wave velocity $C_{SW}$. The azimuthal direction of the propagating front of the wave (direction of the earthquake action) can be arbitrarily specified in the model. At each time of the transient calculation, the distance of each node of the pipeline to the wave front is calculated. As soon as the wave arrives at one point of the pipeline, the three spatial components of the earthquake action are applied simultaneously.

### *4.1 Requirements According to EN 1998-4*

DIN EN 1998-4, appendix B.2 (2010) allows using detailed 3D calculation models however no requirements are made regarding modelling approaches. According to DIN EN 1998-4, section 6.5.2 (2010), for welded steel pipelines maximum strains must not be exceeded in order to ensure deformation compatibility and sufficient buckling resistance. The permissible tensile strain is 3% and the permissible compression strain is the smaller value of 1% and 20 t / R [%].

### *4.2 Further Requirements for Curved Sections*

For pipe sections with strong curvatures, such as those used as “U-strain” curves to compensate for thermal expansion, the calculation must take into account the flexibility and stress intensification. Bending stresses directed parallel to the axis of the bend pipe produce a radially directed stress component, which compresses the outer and inner pipe walls against the neutral axis in a bending moment that increases the bending moment and vice versa. Under the influence of the bending stresses a flattening of the pipe cross-section (ovalization) occurs. This results in lower stresses and a smaller bending moment than in the general bending theory. This correlation is described in the flexibility factor, also known as the Kármán-number: A straight pipe section of length L, diameter D and thickness t will undergo rotation θ as a result of the bending moment M. A curved pipe section with the same diameter D, thickness t and arc length L will experience the curvature k·θ due to the same moment M. Flexibility factors from literature and codes are summarized in Table 1 for 90° bends and they can be used for both, in-plane and out-of-plane bending. The stiffening effect of adjacent straight pipes is included in this factor. For bend angles between 90° and 0 the flexibility factor can be reduced linearly.

Table 1. Flexibility factor k for 90° bend.

| Flexibility factor | According to | Remarks | Characteristics |
|---|---|---|---|
| $\frac{10 + 12 \cdot h^2}{1 + 12 \cdot h^2}$ | Kármán (1911) | Applicable at h > 0.3 | $h = \frac{t \cdot R}{r^2}$ 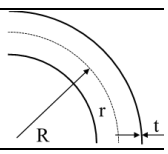  |
| $1.65/h$ | DIN EN 13941 (2010)<br>ASME B31.3 (2010) | Valid for h < 0.33 | |

Similarly, the stress in the curved pipe differs from that in the straight pipe of the same dimension and stress. The stress intensification in the curvature section is then considered by means of appropriate increase factors. According to international codes, different values for in-plane and out-of-plane bending can be used, which are summarized in Table 2.

Table 2. Stress intensification factor i.

| Intensification factor | According to | Remarks | Characteristics |
|---|---|---|---|
| $0.90/h^{\frac{2}{3}} > 1$ | DIN EN 13941 (2010) | In-plane and out-of-plane | $h = \frac{t \cdot R}{r^2}$ 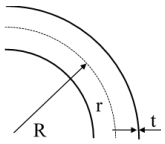  |
| $0.90/h^{\frac{2}{3}} > 1$ | ASME B31.3 (2010) | In-plane | |
| $0.75/h^{\frac{2}{3}} > 1$ | | Out-of-plane | |

## 5 PARAMETER STUDY

The following parameter study is carried out to indicate the influence of several parameters given or assumed in the calculation such as incoming wave angle, wave velocity, soil depth and selected displacement time histories. The example calculations are performed on a 90° bend pipe model with two straight pipe sections, before and after the bend.

### *5.1 Model Parameters*

A steel pipe is regarded with a nominal diameter of DN 250 and a wall thickness of 5 mm. The soil weight is $\gamma$ = 20 kN/m$^3$, the angle of friction of the soil is $\varphi$ = 35°, the pipe material coefficient is f = 0.8 and the coefficient for earth pressure at rest $K_0$ is 1.0. Cohesion c and adhesion $\alpha$ are not considered and the backfill height H above the pipe is chosen to be 2.0 m. The fillet radius between two straight pipe sections is 2.0 m. A single pipe bend is tested with straight sections of 40 m before and after the bend. Pre-tests have shown that this length is sufficient for the seismic load application. Longer straight sections did not result in significantly higher pipe stresses. The model is displayed in Figure 9. For the analyses von Mises stresses were evaluated.

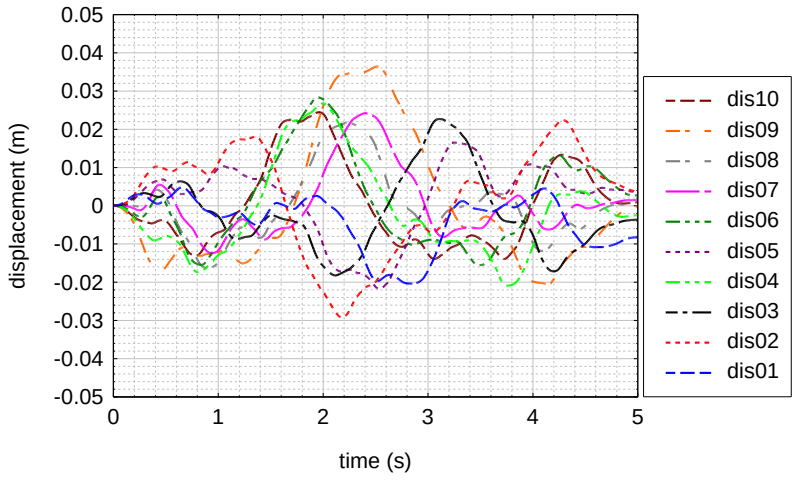


Figure 7. Synthetic displacement time histories

As seismic load requirement, the horizontal response spectrum from DIN EN 1998-1 / NA (2010) for the underground combination C-T (intermediate deep sediments) was used and scaled to a peak ground acceleration (PGA) of 1 m/s$^2$. For the vertical seismic action, 50 % of the horizontal load was applied. The duration of the time histories was chosen to 5 s. Spectrum compatible and stochastically

independent displacement time histories were generated, all time histories were baseline corrected. The displacement time histories are shown in Figure 7. The maximum ground displacement (PGD) is almost 3 cm. Figure 8 shows the acceleration response spectra of the generated time histories together with the target spectrum to visualize the quality of approximation.

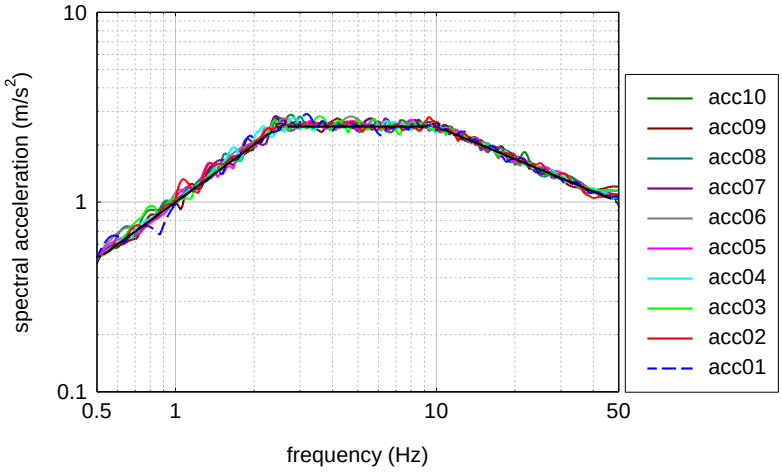


Figure 8. Horizontal response spectra (5 % damping) of the synthetic time histories in Figure 7 and target spectrum from DIN EN 1998-1/NA (2010)

### *5.2 Variation of Azimuthal Wave Direction*

For the model with the 90° bend, the incident angle of the earthquake wave front to the x-axis was varied. The angles 0° (in the axis of the first pipe section), 22.5°, 45°, 77.5°, 90°, 112.5°, 135° and 157.5° were evaluated (see Figure 9).

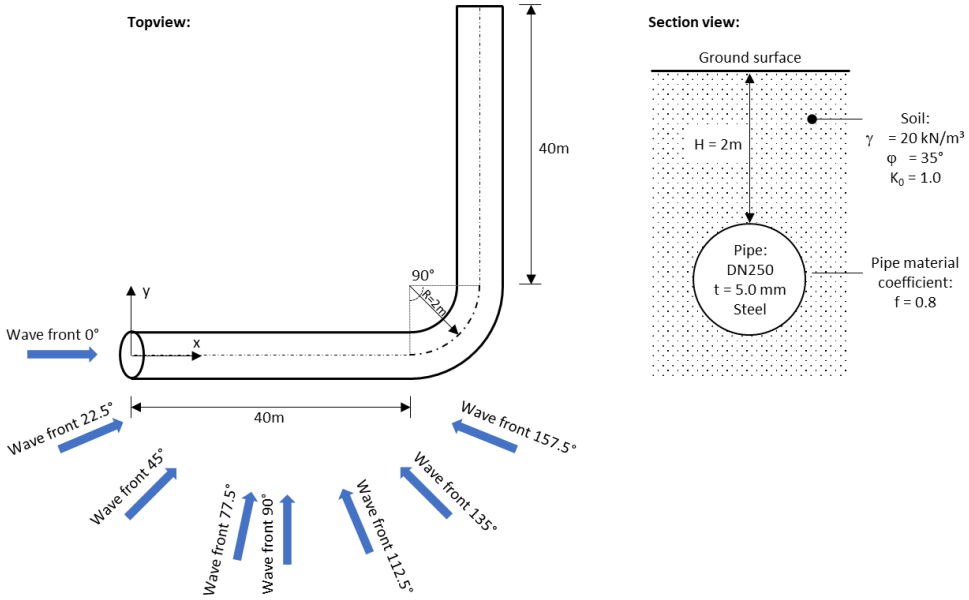


Figure 9. Calculation example and evaluated incident angles of the earthquake wave front

In this example, only the x component of the displacement time histories is applied. This ensures, that the mutual influence of the time profiles has no effect on the results. The ratio of the maximum stress over each time history to the maximum stress of all calculation runs is shown in Figure 10. The greatest

stresses of all considered variants occurred in the model with an incident wave angle of 77.5°. However, further test calculations did not show a most unfavorable incident angle, but indicated that the results depend on the selected synthetic time histories.
The example shows that the incident wave angle, i.e. the azimuthal wave direction of the earthquake, has a significant impact on the results. In practice, there are almost always pipe sections with several changes of direction. Since the worst angle of the incidence wave front is not known a priori, it is recommended to carry out calculations for varying angles.

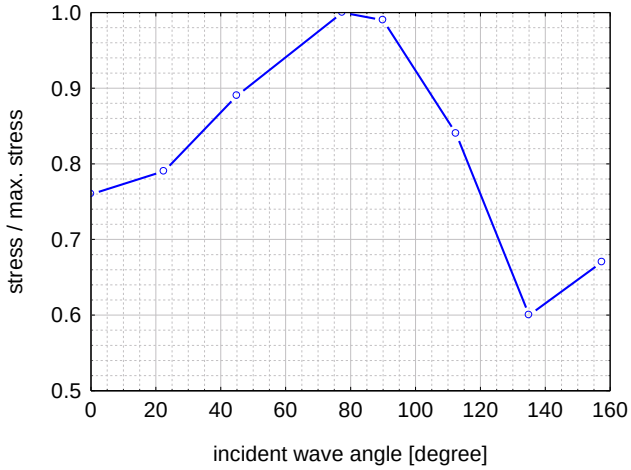


Figure 10. Max. stresses (normalized) dependent on the incident wave angle (model 90° bend)

### *5.3 Variation of Depth*

In the following calculations, the model with the 90° bend is used to examine the influence of the backfill height over the pipeline. The backfill height influences the stiffness of the vertical soil springs. For the calculations, the angle of the incidence wave front is set to 0°. The results standardized to the maximum stress are shown in Figure 11. It can be seen, that the maximum stresses increase with increasing backfill height and asymptotically approach a limit. The increase of the stress is due to the higher transmittable spring forces at larger backfill heights.

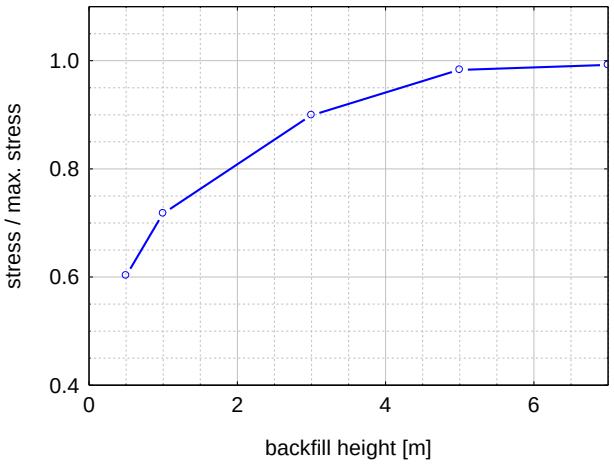


Figure 11. Max. stresses (normalized) dependent on the backfill height (model 90° bend)

### *5.4 Variation of Apparent Wave Velocity*

In further calculations, the apparent wave velocity $C_{SW}$ was varied for the 90° bend model. In addition to realistic wave velocities in the range between 2000 m/s and 5000 m/s (see Section 3), much lower wave velocities were investigated too. Figure 12 shows the results for the considered pipe bend compared to a straight pipe section. For the straight pipe section, the maximum stresses decrease significantly with increasing apparent wave velocity. This is because the straight pipe section experiences very little displacement differences due to the small time offset along the pipeline at higher wave velocities. In the case of a pipe bend the influence of the apparent wave velocity on the stresses is small, as the different spring stiffness in the longitudinal and transversal directions lead to different displacements of the two pipe sections, resulting in higher stresses in the bend. This effect occurs at both higher and lower wave velocities. If an identical stiffness is applied in the longitudinal and transversal direction, it will result in a significant decrease of stresses with increasing wave velocity, like it was observed with the straight pipe section before.

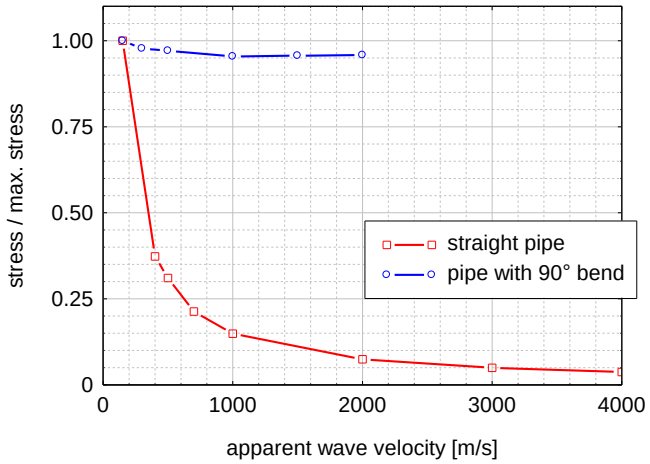


Figure 12. Max. stresses (normalized) dependent on the apparent wave velocity (model 90° bend, straight pipe)

### *5.5 Variation of Peak Ground Displacement*

The scaling of the maximum ground displacement (PGD) as a seismic load requirement means a scaling of the displacement amplitudes of the time histories. Figure 13 shows the influence of PGD on the maximum pipe stresses. For the investigated model with the 90° bend, the stresses above a soil displacement of 10 cm reach a threshold value. This is because after a certain threshold displacement, the pipe slides along the ground. Thus, no higher frictional forces can be transmitted.

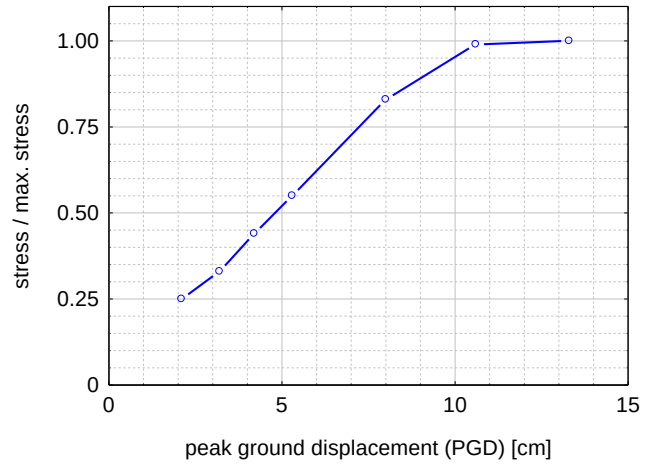


Figure 13. Max. stresses (normalized) dependent on PGD (model 90° bend)

### *5.6 Variation of Synthetic Time Histories*

In the following the influence of synthetic time histories on the results is examined. Again, we use the model of the 90° bend. In a first step, the ten displacement time histories in Figure 7 are applied as x-component in the pipe axis direction (wave front 0°). The normalized deviations from the mean value of the max. stresses of all calculations are plotted in Figure 14. The mean value is 0.82 of the maximum stress. The standard deviation from all calculations is 0.10 and the 95 % quantile is 0.98 of the maximum stress.

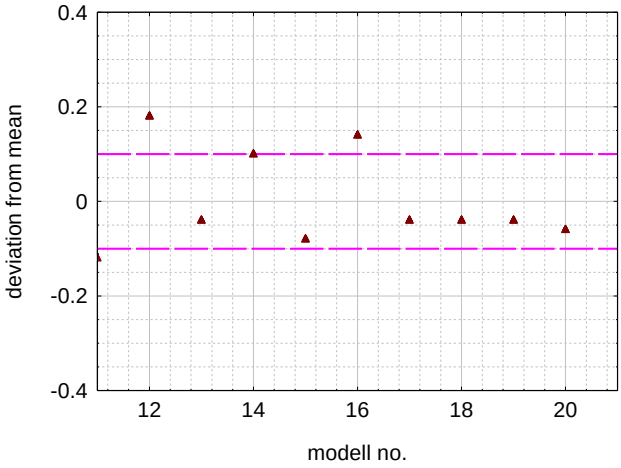


Figure 14. Variation of max. stresses due to different time histories (only x-component): deviation from mean of max. stresses (normalized) and standard deviation (dashed line), (model 90° bend)

In a second step, all three components of the seismic action are applied. From the ten displacement time histories in Figure 8, 20 sets of three components (x, y, z) are grouped by permutation. The vertical component is applied as half of the horizontal components. The results, again given as a deviation from the mean, are shown in Figure 15. In comparison to the previous example, the results show a slightly higher standard deviation of 0.12. The 95 % quantile is 0.98 times the maximum stress as before. The mean value is 0.70 of the maximum stress. According to DIN EN 1998-1, clause 4.3.3.4.3 (3) (2007), at least three sets (of three directional components) of time histories are used from which the maximum resulting values have to be used for design. For the present example, the evaluation of the maximum stresses from three arbitrary chosen calculations result in a stress which corresponds approximately to the mean value plus one standard deviation from all 20 performed calculations.

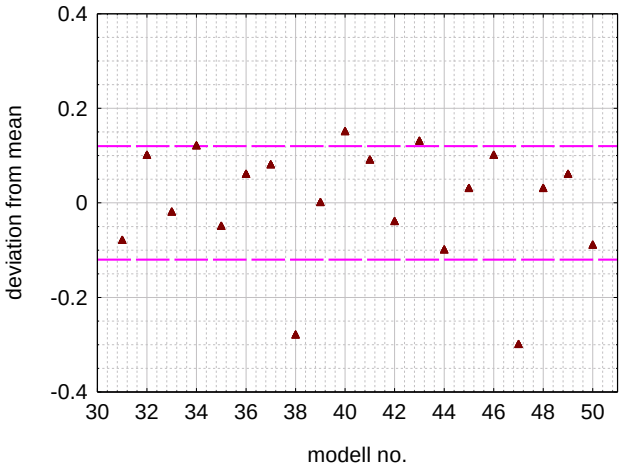


Figure 15. Variation of max. stresses due to different sets of time histories (x, y, z-component): deviation from mean of max. stresses (normalized), standard deviation (dashed line), (model 90° bend)

## 5. CONCLUSIONS

The seismic analyses of underground pipelines as spatially extended structures are influenced by several parameters. The article investigates the influence of the following parameters on the results of pipeline analyses: incoming wave angle, wave velocity, backfill height and synthetic displacement time histories. The results show that stresses of underground pipelines can strongly depend on these parameters. An a priori conservative estimation of the expected stress levels is quite difficult due to the large variation of input parameter. Therefore, it is recommended to apply probabilistic calculation approaches, which considers the variation of all relevant parameters by representative statistical distributions. However, at least variant calculations should be carried out to obtain a reliable design basis for underground pipelines.

## 7. REFERENCES


ALA (2001). Guidelines of the Design and Buried Steel Pipe, *American Lifelines Alliance*.

ASCE (1984). Guidelines for the seismic design of oil and gas pipeline systems, *Technical Council on Lifeline Earthquake Engineering*.

ASME B31.1 (2010). Pressure Piping, Power Piping, *Standard*, American Society of Mechanical Engineers.

Butenweg Ch, Schmitt T, Rosen B (2014). Seismische Einwirkungen auf erdverlegte Rohrleitungssysteme, *Bauingenieur*, 89: 316-324.

DIN EN 1998-1 (2010). Eurocode 8: Design of structures for earthquake resistance – Part 1: General rules, seismic actions and rules for buildings; German version EN 1998-1:2004 + AC:2009.

DIN EN 1998-1/NA (2011). National Annex – Nationally determined parameters – Eurocode 8: Design of structures for earthquake resistance – Part 1: General rules, Seismic actions and rules for buildings.

DIN EN 1998-4 (2006). Eurocode 8: Design of structures for earthquake resistance – Part 4: Silos, tanks and pipelines; German version EN 1998-4:2006

DIN EN 13941 (2010): Design and installation of preinsulated bonded pipe systems for district heating; German and English version EN 13941:2009+A1:2010

EQE (1995). The January 17, 1995 Kobe Earthquake - An EQE Summary Report, *EQE International*, San Francisco, USA.

Kármán Th v (1911). Über die Formänderung dünnwandiger Rohre, insbesondere federnder Ausgleichsrohre, *VDI-Z*, 55: 1889-1895.

Kuhlmann W (2004). Gesamtkonzept zur Ermittlung der seismischen Vulnerabilität von Bauwerken am Beispiel unterirdischer Rohrleitungen, *Ph.D. Thesis*, Faculty of Civil Engineering, RWTH-Aachen University, Germany.

O´Rourke MJ, Bloom MC, Dobry R (1982). Apparent propagation velocity of body waves, *Earthquake Engineering and Structural Dynamics*, 10(2): 283-294.